PCCP

Accepted Manuscript

ROYAL SOCIETY OF CHEMISTRY

www.rsc.org/pccp

Physical Chemistry Chemical Physics
CREATED USING THE RSC LaTeX PCCP ARTICLE TEMPLATE – SEE www.rsc.org/electronicfiles FOR DETAILS
ARTICLE TYPE www. rsc.org/xxxxxx | XXXXXXXX

Infrared spectra of small anionic water clusters from density functional theory and wavefunction theory calculations†

Zu-Yong Gong,[a,b] Sai Duan,*[b] Guangjun Tian,[b] Jun Jiang,[a] Xin Xu,*[c] and Yi Luo[a,b]

Received Xth XXXXXXXXXX 20XX, Accepted Xth XXXXXXXXX 20XX
First published on the web Xth XXXXXXXXXX 200X
DOI: 10.1039/b000000x

We performed systematic theoretical studies on small anionic water/deuterated water clusters $W/D^-_{n=2-6}$ at both density functional theory (B3LYP) and wavefunction theory (MP2) levels. The focus of the study is to examine the convergence of calculated infrared (IR) spectra with respect to the increasing of the number of diffuse functions. It is found that at the MP2 level for larger clusters ($n = 4-6$), only one extra diffuse function is needed to obtain the converged relative IR intensities, while one or two more sets extra diffuse functions are needed for smaller clusters. Such behaviour is strongly associated with the convergence of the electronic structure of corresponding clusters at the MP2 level. It is striking to observe that at the B3LYP level, the calculated relative IR intensities for all the clusters under investigations are diverse and show no trend of convergence when increasing the numbers of the diffuse functions. Moreover, the increasing contribution from the extra diffuse functions to the dynamic IR dipole moment indicates that the B3LYP electronic structure also fails to converge. These results manifest that MP2 is a preferential theoretical method, as compared to the widely used B3LYP, for the IR intensity of dipole bounded electron systems.

1 Introduction

Anionic water clusters (W^-_n) were first detected by mass spectrometry in the early 1980s,[1,2] and have attracted great attention in many areas[3–7] since then. There are two kinds of structure for W^-_n: interior structure and surface structure.[8] In the latter structure, which is preferential for small W^-_n,[8] the excess electron is bounded outside the molecular kernel through the dipole-electron interaction.

To identify structures of W^-_n, diverse optical methodologies including photoelectron,[9] vibrational induced autodetachment[10] and fragmentation[11], vibrational predissociation,[12,13] and time-resolved photoelectron[14,15] spectroscopies have been used. Among them, vibrational predissociation spectroscopy which avoids the so-called "Fano" resonance as well as continuum background[16] can provide high resolution of "fingerprint" vibrational information that is equivalent to the corresponding infrared (IR) spectrum. The high resolution IR spectrum of W^-_6 in the OH stretching region was first observed by vibrational predissociation spectroscopy in 1998.[12] In addition, to further circumvent the continuum background, anionic deuterated water clusters D^-_n were used to detect the IR spectra for D^-_3 in the DOD bending region[17] and D^-_{4-6} in the OD stretching region[13]. Besides, the IR spectra of partially deuterated anionic water hexamers were also reported in the literature.[18]

Because of rapidly increasing number of isoenergetic conformers with the size of W^-_n,[19,20] theoretical investigations are essential for identifying their structures. The theoretical fundamental of W^-_n in the surface state could be traced back to the quantum theory of an electron in the field of a finite dipole.[21] In such case, the value of the dipole moment should be larger than 1.625 Debye to bound an extra electron.[22–26] If further considering the electronic-rotational coupling, it has been proved that the critical value is dependent on the moments of inertia of the molecule.[27] Thus, for real molecules that are free to rotate, the critical dipole moment is in the range from 2.0 to 2.5 Debye.[27,28] Notice that, neutral water monomer has dipole moment around 1.85 Debye,[29] which is larger than the critical value (1.625 Debye) for bounding an extra electron if it is fixed but smaller than the critical value if it is freely rotating. Thus, water monomer even in its lowest rotational level would not bind an extra electron and there was no experimental evidence for it. Indeed, previous theoretical investigations showed that a single water molecule at or near its equilibrium geometry does not have the ability to capture

† Electronic Supplementary Information (ESI) available: Calculated IR spectra with other DFT functionals. See DOI: 10.1039/b000000x/

[a] *Hefei National Laboratory for Physical Sciences at the Microscale, Department of Chemical Physics, School of Chemistry and Materials Science, University of Science and Technology of China, Hefei, Anhui 230026, P. R. China*
[b] *Department of Theoretical Chemistry and Biology, School of Biotechnology, Royal Institute of Technology, S-106 91 Stockholm, Sweden. E-mail: said@theochem.kth.se*
[c] *Collaborative Innovation Center of Chemistry for Energy Materials, Shanghai Key Laboratory of Molecular Catalysis and Innovative Materials, MOE Laboratory for Computational Physical Science, Department of Chemistry, Fudan University, Shanghai, 200433, P. R. China. E-mail: xxchem@fudan.edu.cn*

Table 1 Exponents of diffuse functions.

	m,n	O_s	O_p	H_s
P*mn*D				
	1	0.0105625000000	0.0105625000000	0.0045000000000
	2	0.0013203125000	0.0013203125000	0.0005625000000
	3	0.0001650390625	0.0001650390625	0.0000703125000
A*mn*D				
	1	0.0092200000000	0.0074675000000	0.0031575000000
	2	0.0011525000000	0.0009334375000	0.0003946875000
	3	0.0001440625000	0.0001166796875	0.0000493359375
S*mn*D				
	1	0.0112537500000	0.0079812500000	0.0040500000000
	2	0.0014067187500	0.0009976562500	0.0005062500000
	3	0.0001758398437	0.0001247070313	0.0000632812500

an extra electron through its dipole.[30,31]

Although the *ab initio* calculations for $W^-_{1,2}$ were prior to the experimental observation,[30,32] the theoretical IR investigations were initiated in 1999,[18] shortly after the observation of the high resolution experimental spectra.[12] For theoretical IR spectra, density functional theory (DFT) and wavefunction theory (WFT) have been widely used although the former overestimates and the latter (at the Møller-Plesset second order perturbation (MP2)[33] level) underestimates the vertical electron-detachment energy (VDE) of W^-_n.[34,35] For DFT, the Becke's three-parameters exchange and Lee-Yang-Parr correlation hybrid functional (B3LYP)[36] was most popular[13,18,20,34,37–44] because of its reliable frequency shifts. Through the comparison of the theoretical IR spectra at the B3LYP level with experimental observations, the structures of W^-_{4-6} were found to be 4Rf, 5W3f, and 6Af, respectively.[13,34] Here we followed the terminology proposed by Kim and coworkers.[34] In these structures, a common motif of "free" water is highlighted for capturing the extra electron (see Fig. 1 for details). For WFT, at the MP2 level, the IR spectra of $W^-_{3-5,7}$ were predicted.[34,45] In addition, the structure of D^-_3 was identified as 3L by comparing the calculated (at the MP2 and coupled-cluster singles and doubles (CCSD)[46] levels) and measured IR spectra in the bending region.[17] Moreover, the calculated potential energy surface at the MP2 level reveals the quantum probabilistic structure of W^-_2 is a 2CsI structure which is the transition state between two stable conformers.[47]

The systematic investigations for the calculated VDEs including their convergence with respect to the diffuse functions have been performed.[48–50] However, to the best of our knowledge, there was no convergence study for the IR spectra with respect to the diffuse functions although it is more important for the structures of small W^-_n. We should emphasize here, because the low-lying isoenergetic conformers of W^-_n and their spectral similarity, the systematic investigation for the IR spectra is remarkably indispensable. For instance, the structure of W^-_6 was first assigned as the "tweezerslike",[37] then the linear network,[18] and finally the 6Af[13,34]. During the evolution, the improvement of theoretical spectra played the crucial role. Therefore, in this work, the convergence of IR spectra for W/D^-_{2-6} with respect to the diffuse functions is performed. The convergence of dynamic IR dipole moment is also studied, which allows us to inspect the convergence of electronic structures.

2 Computational Details

For anionic species, diffuse basis sets are important for the first principles calculations.[48,51–53] Here, we used three basis sets of triple zeta quality for W^-_n: the Pople's 6-311++G(d,p),[54,55] the augmented Dunning's correlation consistent basis set aug-cc-pVTZ with Davidson's linear transformation for contraction,[56–58] and the Sadlej's polarized basis set[59]. Based on these basis sets, up to three sets of diffuse function were added. They were labeled as P*mn*D, A*mn*D, and S*mn*D with $m,n = 0,1,2,3$, respectively. Here m and n represent the number of s and p diffuse functions for oxygen and the number of s diffuse function for hydrogen, respectively. Meanwhile, the corresponding exponents used the scaled values of the outermost exponents by 0.125 consecutively.[34] Specifically, all used exponents were listed in Table 1. We should emphasize that the scheme of diffuse functions was widely used for W^-_n. For instance, P10D is the 6-311++G(d,p)+diff(sp) used in Ref. 13 for exploring the structures of W/D^-_{4-5} and A22D is the aug-cc-pVTZ+diff($2s2p/2s$) used in Ref. 45 for calculating the VDEs of W^-_{3-5}.

The B3LYP functional[36] was chosen for DFT, while, MP2[33] for WFT. As mentioned before, there was no existence of W^-_1. Thus, here we did not consider this species.

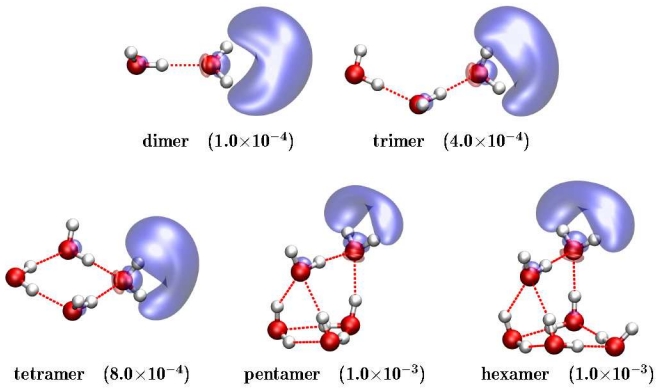

Fig. 1 Optimized anionic water clusters and their MP2 spin density at the MP2/S33D level. The values in parenthesis are the corresponding iso-values for the MP2 spin density.

The most probable conformers for W_{2-6}^- related to the experimental observation were considered. Followed by the terminology proposed by Kim and co-workers,[34] they are 2CsI, 3L, 4Rf, 5W3f, and 6Af, respectively. All degrees of freedom of the clusters were optimized at corresponding theoretical levels and all optimized structures at the MP2/S33D level were depicted in Fig. 1. Besides, the distributions of extra electron shown in Fig. 1 demonstrate all species are dipole bounded systems. The pruned "ultrafine" grids were used for numerical integrations in DFT. Our test calculate showed that the total energy converges to 10^{-6} a.u. when more intense "superfine" grids were used. The calculated expectation values of the total spin angular momenta ($\langle S^2 \rangle$) for all species were 0.75 indicating no spin contamination in the calculations. The analytical frequency calculations were performed to confirm that each geometry is a true local minimum except W_2^-. As mentioned before, W_2^- is a transition state which has only one imaginary frequency. Unfortunately, we could not locate the 2CsI structure at the B3LYP level as well as the MP2/A*mn*D level.[34] As a result, we used the optimized geometries with corresponding aug-cc-pVDZ+diff basis sets[47] instead of A*mn*D at the MP2 level and did not consider it for B3LYP. The calculated IR intensities were broadened by the Lorentzian function and the frequencies were scaled properly to facilitate comparison with the experimental counterparts. The specific full width at the half-maximum (fwhm) for Lorentzian function as well as scaling factors were given in the following individually. All electronic structure calculations were performed with Gaussian 09 suite of programs.[60]

In both DFT and WFT, the dipole moment could be calculated as

$$\mu = -\mathrm{Tr}(PX) + \sum_A Z_A R_A, \qquad (1)$$

where P is the generalized one-particle density matrix, X is the multipole matrix, Z_A is the nuclear charge for atom A, and R_A is the corresponding Cartesian coordinates. The dynamic IR dipole moment of the k-th normal mode ($d\mu_k$) could be calculated from the direct differentiation of dipole moment, *i.e.*,

$$d\mu_k = \frac{\partial \mu}{\partial Q_k} = -\mathrm{Tr}\left(\frac{\partial P}{\partial Q_k}X + P\frac{\partial X}{\partial Q_k}\right) + \sum_A Z_A \frac{\partial R_A}{\partial Q_k}. \qquad (2)$$

The second term in Eq. 2 represents the nuclear contribution to $d\mu_k$. Notice that the Tr would run over all basis set index, thus, the electronic contribution for $d\mu_k$ in Eq. 2 (the first term) could be easily decomposed to each atomic orbitals. In other words, $d\mu_k$ could be decomposed to different components, *i.e.*, nuclear, core, valence, polarization, and diffuse. The analytical calculations of $\partial X/\partial Q_k$ and $\partial R_A/\partial Q_k$ are straightforward.[61–63] On the other hand, for $\partial P/\partial Q_k$, it could be also calculated from the couple-perturbed method analytically.[64,65] However, for the MP2 method, we obtained it numerically by the central finite difference method[66] with $\Delta Q_k = \pm 1.0 \times 10^{-3}$. Finally, the projection of all components along the direction of total $d\mu_k$ was calculated. It is noted that current scheme focuses on the basis set decomposition for $d\mu_k$, which is different from the methods based on atomic polar tensors.[67–69] In principle, this scheme is in the framework of Mulliken population analysis[70] and can be easily extended for the non-resonant Raman intensities.[71]

3 Results and Discussions

3.1 Dimer

We start our study from W_2^- which is the simplest species of W_n^- observed by experiments.[9] Although there were no experimental IR spectra available for W_2^-, we could benefit from its theoretical IR spectra because they are much simpler than the other larger W_n^-.

As mentioned before, here we only considered W_2^- at the MP2 level. Notice that there is a blue shift in frequency in both the bending and stretching regions when adding extra diffuse functions. The blue shift is also observed for other W_n^- and also at the B3LYP level. By increasing the number of diffuse functions, the calculated IR spectra nearly converged with three sets of extra diffuse functions as shown in Fig. 2. To analyze $d\mu_k$, we select two vibrational modes involving the "free" water, namely: ν_b in the bending region and ν_s in the stretching region. In the bending region, the HOH bending mode (ν_2) of the "free" water is less mixed with those from other water molecules. Thus, here, ν_b represents the ν_2 mode of the "free" water. On the other hand, in the stretching region, the mode mixing is significant for the symmetrical OH stretching modes (ν_1) of the "free" water. We define ν_s as the symmetrical mixing of the ν_1 modes involving the "free" water. The other two important modes, labeled as ν_s' and ν_a hereafter, are

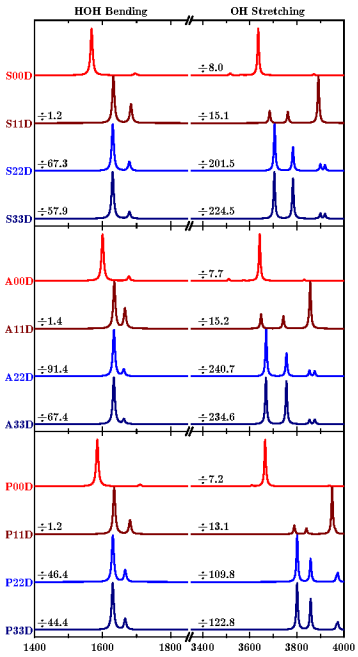

Fig. 2 Calculated IR spectra for anionic water dimer at the MP2 level. All calculated spectra were broadened by a Lorentzian function with a fwhm of 7.5 cm^{-1}. The values are the corresponding scale factor for the spectra with respect to the maximum intensity in the bending region with S00D, A00D, and P00D, respectively.

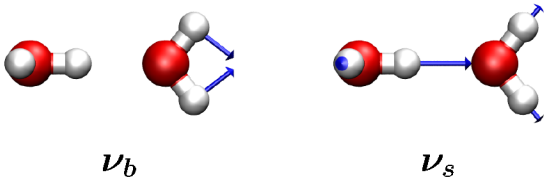

Fig. 3 Schematic vibrational modes for ν_b and ν_s.

the anti-symmetrical mixing of ν_1 involving the "free" water and the non-mixing anti-symmetrical OH stretching mode (ν_3) of the "free" water. ν_b and ν_s always appear at the lowest band in the corresponding region and their schematic drawing were depicted in Fig. 3. It should be noticed that, usually, ν_s has less proportion of the "free" water, while, ν_s' has more proportion. In the bending region of the calculated IR spectra of W_2^-, calculations with all three sets of extra diffuse functions show that ν_b is the most intense band. In the stretching region, ν_s and ν_s' both have significant intensities, while the contribution of ν_a could be negligible.

The detailed analysis of $d\mu_k$ for W_2^- are listed in Table 2. The contribution from diffuse functions dominates $d\mu_k$ when more than two sets are added. Both the outermost and the second outermost diffuse functions have significant contributions in $d\mu_k$ with the most diffuse basis sets. On the other hand, the contribution from diffuse function only has minor variation. In addition, the calculated VDE at the MP2/S33D level is 0.018 eV, which confirms that W_2^- is stable. These results are consistent with the experimental observation[9] of W_2^-. Consequently, the MP2 level with the most diffuse basis sets used here has the ability to describe the extra electron in W_2^- because the calculated IR spectra almost converged (only a small variation of ν_s' shown in Fig. 2). It is nice to see that the calculated IR spectra with S*mn*D are similar to their counterparts with A*mn*D shown in Fig. 2 (even the two high frequency bands in the stretching region are similar). This result is also consistent with previous theoretical results.[51,72,73] Therefore, for larger $W_{n\geq 3}^-$, only S*mn*D and P*mn*D are used in order to

Table 2 Components of dynamic IR dipole moment for anionic water dimer. N: Nuclear; C: Core basis set; V: Valence basis set; P: Polarization basis set; D: Diffuse basis set; T: Total.

m,*n*	N	C	V	P	D	T
			ν_b			
S*mn*D						
00	-0.49	-0.04	-0.54	-0.26	2.11	0.78
11	-0.11	-0.01	-0.08	0.05	1.00	0.85
22	0.50	0.05	0.10	-0.15	5.94	6.44
33	0.51	0.05	0.10	-0.15	5.49	5.99
A*mn*D						
00	-0.50	-0.12	0.65	0.05	0.75	0.82
11	-0.01	0.00	0.03	0.00	0.95	0.96
22	0.50	0.12	-0.44	-0.02	7.71	7.88
33	0.51	0.13	-0.45	-0.02	6.55	6.72
P*mn*D						
00	-0.47	-0.06	0.42	0.09	0.78	0.76
11	-0.25	-0.03	0.04	0.05	1.02	0.83
22	0.55	0.07	-0.23	-0.08	4.86	5.18
33	0.55	0.08	-0.24	-0.08	4.75	5.07
			ν_s			
S*mn*D						
00	0.34	0.03	0.81	-0.29	-0.44	0.45
11	0.36	0.04	-0.26	0.01	1.41	1.57
22	0.45	0.05	-0.15	0.08	10.74	11.16
33	0.45	0.05	-0.14	0.08	11.21	11.64
A*mn*D						
00	0.39	0.10	0.33	-0.11	-0.26	0.44
11	0.35	0.09	0.03	-0.15	1.49	1.80
22	0.45	0.11	0.15	-0.22	12.29	12.78
33	0.46	0.11	0.15	-0.22	12.08	12.59
P*mn*D						
00	0.24	0.03	-0.46	0.12	0.39	0.31
11	0.32	0.04	-0.37	-0.04	1.23	1.19
22	0.45	0.06	-0.39	-0.08	7.93	7.98
33	0.46	0.06	-0.40	-0.08	8.37	8.42

Table 3 Components of dynamic IR dipole moment for anionic water trimer. N: Nuclear; C: Core basis set; V: Valence basis set; P: Polarization basis set; D: Diffuse basis set; T: Total.

	MP2						B3LYP					
m,n	N	C	V	P	D	T	N	C	V	P	D	T
						ν_b						
SmnD												
00	0.00	-0.06	-0.89	0.03	1.38	0.48	0.00	-0.06	-0.86	0.01	1.31	0.41
11	-0.01	0.08	0.81	-0.18	-0.22	0.48	0.00	-0.03	0.01	-0.02	0.18	0.14
22	-0.01	0.08	0.82	-0.18	0.04	0.75	0.00	0.00	0.17	-0.03	17.89	18.03
33	-0.01	0.08	0.82	-0.18	0.03	0.75	0.01	-0.07	-0.99	0.20	2.68	1.83
PmnD												
00	0.00	-0.09	0.19	0.07	0.30	0.47	0.00	-0.08	0.04	0.06	0.34	0.36
10	0.00	-0.07	0.04	0.06	0.23	0.27	0.01	-0.10	0.01	0.07	0.41	0.40
11	-0.01	0.11	0.00	-0.06	0.30	0.34	0.01	-0.10	0.04	0.07	0.10	0.12
22	-0.01	0.13	-0.02	-0.07	0.97	1.00	0.00	-0.06	0.00	0.07	1.84	1.85
33	-0.01	0.13	-0.02	-0.07	0.98	0.98	0.00	0.05	0.03	-0.03	2.64	2.68
						ν_s						
SmnD												
00	0.00	0.01	-0.08	-0.24	0.62	0.30	0.00	-0.03	-0.45	-0.14	1.01	0.40
11	-0.01	0.07	0.73	0.06	1.10	1.96	-0.01	0.07	0.74	0.08	0.64	1.53
22	-0.01	0.07	0.75	0.05	1.99	2.85	0.00	-0.04	-0.15	0.04	32.53	32.38
33	-0.01	0.07	0.75	0.05	1.97	2.85	-0.01	0.08	1.12	0.08	21.87	23.14
PmnD												
00	0.00	0.01	-0.13	0.01	0.38	0.26	0.00	-0.05	0.44	-0.09	0.12	0.42
10	-0.01	0.09	-0.27	0.04	0.90	0.76	0.00	0.08	-0.57	0.06	1.13	0.69
11	-0.01	0.10	-0.24	0.02	1.55	1.43	0.00	0.09	-0.64	0.06	1.76	1.26
22	0.00	0.11	-0.26	0.02	3.00	2.86	0.00	-0.09	0.32	0.01	5.42	5.66
33	-0.01	0.11	-0.26	0.02	2.98	2.84	0.00	-0.03	0.34	-0.06	5.40	5.66

save computational costs. Furthermore, only ν_b and ν_s are analyzed in detail for $d\mu_k$ in the following.

3.2 Trimer

D_3^- is the smallest W/D_n^- for which the experimental IR spectrum has been reported.[17] Because of the low VDE, only the IR signal in the bending region was recorded. Nevertheless, it provides a good reference to validate the theoretical predictions.

All calculated IR spectra for D_3^- as well as the experimental results[17] were depicted in Fig. 4. At the MP2 level, convergence were reached for the relative IR spectra after two extra diffuse function were added in the calculations. The converged spectrum with SmnD agrees well with previous theoretical predictions at the CCSD/aug-cc-pVDZ($2s2p/2s$) level in Ref. 17. Furthermore, it is also in good agreement with the experimental spectrum in the bending region, where the most intense band is contributed by ν_2 of the other two water molecules rather than that of the "free" water. These results indicate that the correlation is adequate for IR at the MP2 level, although MP2 underestimates the VDEs.[34,35] On the other hand, the converged IR spectrum with PmnD overestimates the intensity of ν_b which becomes the most intense one in the bending region. This result reveals that SmnD are better than PmnD for IR simulations. In the stretching region, there are three significant bands. Specifically, they are ν_s, ν_s' and ν_a from low to high frequency. As compared with the spectra of W_2^-, ν_a is more clear in D_3^-.

The components of $d\mu_k$ for D_3^- listed in Table 3 are fully converged after two sets of extra diffuse functions were added, which is consistent with the convergence of the relative intensities shown in Fig. 4. The contribution of the diffuse functions dominates $d\mu_k$ for the converged results except for the ν_b mode with SmnD. Surprisingly, the dominant component for ν_b with S33D is the valence part. This result should be attributed to the cancellation of the contribution from diffuse functions. In fact, the second outermost diffuse functions have the largest absolute value in $d\mu_k$. The full convergence of all components reveals that the electronic structure of the extra electron in D_3^- has been adequately described by the MP2 method with two sets of extra diffuse functions. Here the nu-

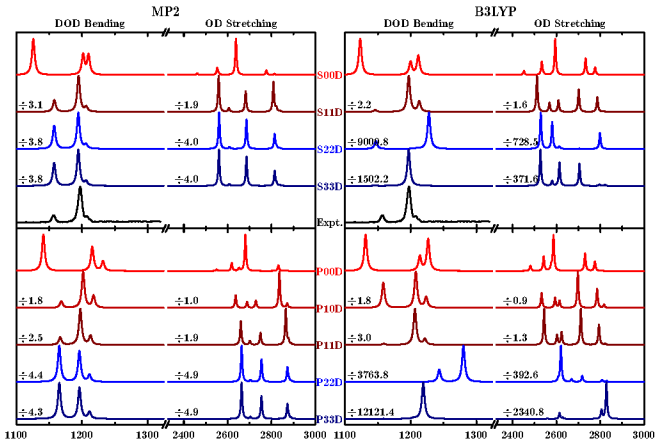

Fig. 4 Calculated IR spectra for anionic water trimer at the MP2 and B3LYP levels. All calculated spectra were broadened by a Lorentzian function with a fwhm of 5.0 cm^{-1} in the bending region and 7.5 cm^{-1} in the stretching region. The frequency scaling factors are 0.97, 0.975, 0.985, and 1.00 in the bending region for the MP2/S*mn*D, MP2/P*mn*D, B3LYP/S*mn*D, and B3LYP/P*mn*D, respectively. The values are the corresponding scale factor for the spectra with respect to the maximum intensity of bending and stretching regions with S00D and P00D, respectively. The experimental IR spectrum in the bending region extracted from Ref. 17 was also included for comparison.

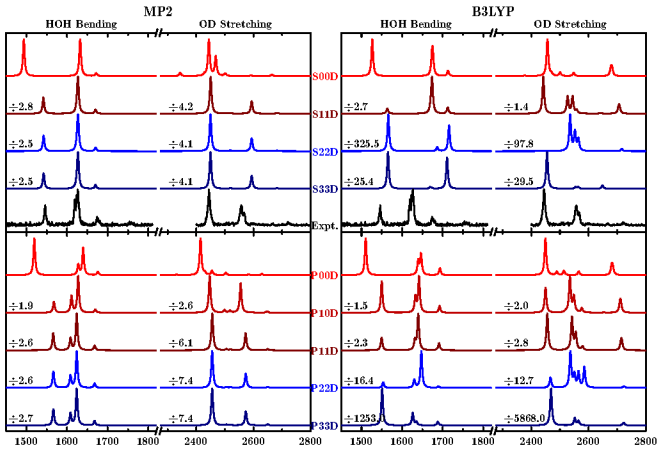

Fig. 5 Calculated IR spectra for anionic water tetramer at the MP2 and B3LYP levels. All calculated spectra were broadened by a Lorentzian function with a fwhm of 5.0 cm^{-1} in the bending region and 7.5 cm^{-1} in the stretching region. The frequency scaling factors are 0.96, 0.96, 1.00, 0.99 in the bending region as well as 0.95, 0.92, 0.97, 0.97 in the stretching region for the MP2/S*mn*D, MP2/P*mn*D, B3LYP/S*mn*D, and B3LYP/P*mn*D, respectively. The values are the corresponding scale factor for the spectra with respect to the maximum intensity of bending and stretching regions with S00D and P00D, respectively. The experimental IR spectra extracted from Ref. 13 were also included for comparison.

clear contributions are all around zero which could be attribute to the fact that the mass ratio between D and O are close to the nuclear charge ration between them in D_n^-. Because of all vibrations are invariant for the center of mass, in this case, the magnitude of the nuclear contributions should be around zero.

The calculated relative intensities for D_3^- at the B3LYP level do not have any trend of convergence as shown in Fig. 4. It is interesting to see that, the result at the B3LYP/P10D level is similar to the converged prediction at the MP2/S*mn*D level in the bending region and seems to reproduce the experimental spectrum reasonably well. However, its large deviation in the stretching region when compared with the MP2/S*mn*D result as well as the unconverged behaviour indicate that such a resemblance is merely a coincidence. This case also highlights the importance of convergence investigation of the present work. Without convergence, comparison between theoretical and experimental results can lead to unreliable interpretations. The components of $d\mu_k$ in Table 3 show that the diffuse functions make a dominant contribution at the B3LYP level. However, their contribution is rather unstable. Therefore, the variance of the calculated IR spectra could be attributed to the questionable description of the extra electron in D_3^- at the B3LYP level, which further confirms the coincidence of the results with P10D. It is noted that, in anionic systems, the extra electron has a tendency of partial ionization because of the self-interaction errors associated with the approximate DFT functionals.[74,75] This situation would be worse for W/D_n^- since the electron is just weakly bounded. We have tested seven more representative DFT functionals for trimer. They are PBE,[76] BPL,[77,78] LC-BLYP,[79] M06-2X,[80] CAM-B3LYP,[81] ωB97XD,[82] and B2PLYP[83] functionals. These functionals contain self-interaction corrected correlation (PL in BPL),[78] different fraction of exact exchange (CAM-B3LYP, M06-2X, ωB97XD, and B2PLYP),[80–83] asymptotic correction by the range-separated method (CAM-B3LYP, LC-BLYP, and ωB97XD),[79,81,82] dispersion corrected functional (ωB97XD),[82] and the nonlocal perturbative correlations (B2PLYP)[83]. Calculated results show that the electronic self-consistent field fails at the M06-2X/S22D level, and geometrical optimizations fail at the PBE/S22D, BPL/S22D, and B2PLYP/S22D levels. Three range-separated functionals can give successful results with all S*mn*D basis sets. However, the convergence of IR spectra is not reached with the CAM-B3LYP (see ESI† for details), although it has two extra parameters for the range-separated algorithm.[81] On the other hand, the calculated IR spectra converged with the LC-BLYP and ωB97XD. We find that the converged IR spectra at the LC-BLYP level in the bending region are similar with that at the MP2 level and, in the stretching region, the results from ωB97XD and MP2 are similar (see ESI† for details). Nevertheless, we also find that the results from LC-BLYP in the

Table 4 Components of dynamic IR dipole moment for anionic water tetramer. N: Nuclear; C: Core basis set; V: Valence basis set; P: Polarization basis set; D: Diffuse basis set; T: Total.

	MP2						B3LYP					
m,n	N	C	V	P	D	T	N	C	V	P	D	T
						ν_b						
SmnD												
00	-0.42	-0.04	-4.80	-1.69	7.74	0.78	-0.46	-0.04	-3.80	-1.83	6.77	0.64
11	0.15	0.01	0.22	0.05	0.43	0.87	-0.29	-0.03	-3.95	-0.91	5.57	0.39
22	0.02	0.00	-1.22	-0.22	2.22	0.80	-0.57	-0.05	-5.95	-1.27	19.39	11.55
33	0.02	0.00	-1.22	-0.22	2.22	0.80	-0.49	-0.04	-5.50	-1.22	10.49	3.24
PmnD												
00	-0.42	-0.06	0.35	0.09	0.78	0.74	-0.44	-0.06	0.15	0.08	0.92	0.64
10	-0.20	-0.03	0.02	0.05	0.72	0.56	-0.44	-0.06	0.03	0.08	1.12	0.73
11	0.25	0.03	-0.19	-0.03	0.75	0.82	-0.36	-0.05	0.08	0.07	0.83	0.56
22	0.22	0.03	-0.18	-0.03	0.75	0.80	-0.50	-0.07	0.18	0.07	1.32	1.01
33	0.23	0.03	-0.18	-0.03	0.75	0.80	-0.39	-0.05	0.08	0.06	22.97	22.66
						ν_s						
SmnD												
00	-0.01	0.06	2.67	-2.09	-0.23	0.41	0.00	0.04	0.35	-0.66	0.44	0.17
11	-0.01	0.09	-0.92	-1.15	4.78	2.79	-0.01	0.07	-0.85	-1.15	3.53	1.59
22	-0.01	0.09	-0.85	-1.14	4.68	2.77	0.00	0.05	-0.40	-0.86	2.56	1.34
33	-0.01	0.09	-0.85	-1.14	4.68	2.77	0.00	-0.05	0.42	0.86	5.99	7.22
PmnD												
00	0.00	0.07	-0.95	0.22	0.85	0.18	0.00	-0.07	1.18	-0.23	-0.78	0.12
10	-0.01	0.12	-1.10	0.24	2.20	1.45	-0.01	0.10	-1.64	0.23	2.23	0.91
11	-0.01	0.12	-1.08	0.22	2.98	2.23	-0.01	0.10	-1.65	0.23	2.63	1.31
22	-0.01	0.12	-1.08	0.22	3.20	2.45	0.00	-0.04	0.90	-0.16	0.78	1.48
33	-0.01	0.12	-1.08	0.22	3.20	2.46	0.00	-0.07	1.16	-0.18	59.14	60.04

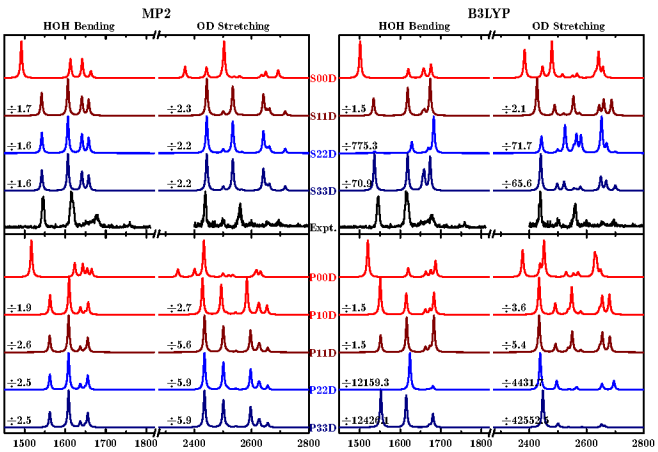

Fig. 6 Calculated IR spectra for anionic water pentamer at the MP2 and B3LYP levels. All calculated spectra were broadened by a Lorentzian function with a fwhm of 5.0 cm^{-1} in the bending region and 7.5 cm^{-1} in the stretching region. The frequency scaling factors are 0.96, 0.96, 0.98, 0.99 in the bending region as well as 0.97, 0.93, 0.975, 0.97 in the stretching region for the MP2/S*mn*D, MP2/P*mn*D, B3LYP/S*mn*D, and B3LYP/P*mn*D, respectively. The values are the corresponding scale factor for the spectra with respect to the maximum intensity of bending and stretching regions with S00D and P00D, respectively. The experimental IR spectra extracted from Ref. 13 were also included for comparison.

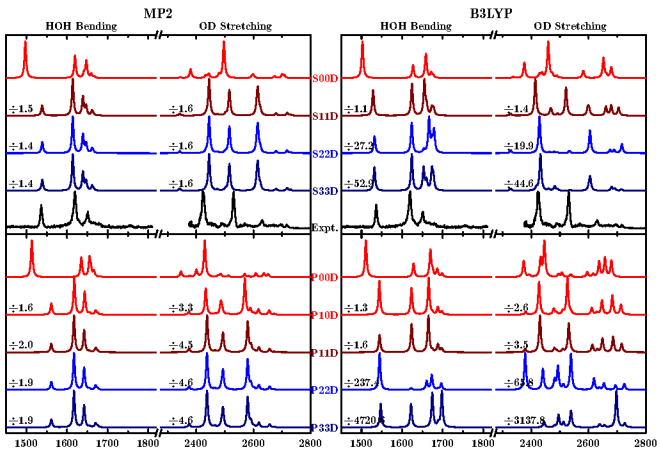

Fig. 7 Calculated IR spectra for anionic water hexamer at the MP2 and B3LYP levels. All calculated spectra were broadened by a Lorentzian function with a fwhm of 5.0 cm^{-1} in the bending region and 7.5 cm^{-1} in the stretching region. The frequency scaling factors are 0.96, 0.96, 0.98, 0.99 in the bending region as well as 0.97, 0.93, 0.97, 0.97 in the stretching region for the MP2/S*mn*D, MP2/P*mn*D, B3LYP/S*mn*D, and B3LYP/P*mn*D, respectively. The values are the corresponding scale factor for the spectra with respect to the maximum intensity of bending and stretching regions with S00D and P00D, respectively. The experimental IR spectra extracted from Ref. 13 were also included for comparison.

stretching region and ωB97XD in the bending region are different from the corresponding MP2 results (see ESI† for details). These results highlight the role of the self-interaction errors for W/D_n^- and encourage us to find the suitable functionals for current systems, which would be our future work.

3.3 Tetramer, Pentamer, and Hexamer

There were high experimental resolution IR spectra for W_{4-6}^- in the bending region and D_{4-6}^- in the stretching region.[13] Here we present our calculation results.

The calculated IR spectra of W_4^- in the bending region and D_4^- in the stretching region were depicted in Fig. 5. At the MP2 level, the relative IR intensities show convergence when only one extra diffuse function was added. The band assignment for S*mn*D and P*mn*D is the same. Specifically, in the bending region of the converged IR spectra, the first band is ν_b as discussed before. The second band, *i.e.* the most intense band, belongs to ν_2 of the two water molecules connected with the "free" water (see Fig. 1 for the details). There are two almost degenerate vibrational modes and the one with slightly higher frequency is much intense than the lower one because of the concerted ν_2 motion of these water molecules. The third band belongs to ν_2 of the water molecule that is the farthest from the extra electron. In the stretching region, there are two bands. The lower band is ν_s and the higher band is ν_a. Here, the intensity of ν_s' is suppressed because of the cancellation from the ν_1 motion. The present assignment is consistent with that in Ref. 13. Although the calculated IR spectra with P*mn*D show splittings in the main band in the bending region, there is no splitting of ν_a in the stretching region. Thus, the two splitting bands observed in experiments would probably be attributed to some other isoenergetic conformers of W/D_4^-. This has also been addressed in the previous investigations for VDEs.[43,84]

The detailed components of $d\mu_k$ for W/D_4^- were listed in Table 4. Although the relative intensities are converged when only one extra diffuse function was added, the absolute value of $d\mu_k$ converges apparently after two sets of extra diffuse function were added. The largest absolute contribution comes from the second outermost *s* diffuse functions of H and O, which is consistent with the convergence of components of $d\mu_k$. Except diffuse functions, other terms also have significant contribution to $d\mu_k$. For instance, the valence functions have negative contribution to the ν_b with S*mn*D and ν_s with P*mn*D, while, both valence and polarization functions contribute to the ν_s with S*mn*D. Here we also noticed that the nuclear component for ν_b with S*mn*D is almost perpendicular to the total $d\mu_k$, while with P*mn*D, it is not.

At the B3LYP level, we find that, with S11D, P10D, and

Table 5 Components of dynamic IR dipole moment for anionic water pentamer. N: Nuclear; C: Core basis set; V: Valence basis set; P: Polarization basis set; D: Diffuse basis set; T: Total.

	MP2						B3LYP					
m,n	N	C	V	P	D	T	N	C	V	P	D	T
						ν_b						
SmnD												
00	-0.46	-0.04	-3.74	-2.15	7.08	0.69	-0.51	-0.04	-2.63	-2.10	5.84	0.56
11	0.12	0.01	-0.21	-0.19	0.96	0.71	-0.33	-0.03	-4.61	-0.93	6.36	0.46
22	0.02	0.00	-1.48	-0.39	2.50	0.65	-0.53	-0.05	-5.72	-1.03	10.83	3.51
33	0.02	0.00	-1.49	-0.39	2.51	0.64	-0.39	-0.03	-3.46	-0.63	9.18	4.67
PmnD												
00	-0.49	-0.07	0.18	0.11	0.91	0.65	-0.52	-0.07	-0.11	0.10	1.14	0.53
10	-0.24	-0.03	0.14	0.05	0.73	0.64	-0.49	-0.07	0.04	0.09	1.07	0.65
11	0.21	0.03	0.01	-0.04	0.50	0.70	-0.39	-0.05	0.09	0.07	0.73	0.44
22	0.15	0.02	0.03	-0.03	0.48	0.66	0.56	0.08	-0.05	-0.10	6.24	6.73
33	0.15	0.02	0.03	-0.03	0.49	0.66	-0.26	-0.04	0.11	0.05	59.35	59.21
						ν_s						
SmnD												
00	0.00	0.00	1.35	-0.47	-0.16	0.73	0.00	-0.02	-0.01	0.02	0.99	0.98
11	0.00	0.04	1.39	-0.10	0.70	2.01	0.00	0.03	0.85	0.02	0.71	1.61
22	0.00	0.04	1.42	-0.11	0.62	1.97	0.00	-0.05	-0.29	0.25	6.48	6.40
33	0.00	0.04	1.42	-0.11	0.62	1.97	0.00	-0.04	-1.17	0.04	10.22	9.05
PmnD												
00	0.00	0.00	-0.74	0.12	1.18	0.56	0.00	-0.05	0.04	-0.01	0.93	0.91
10	0.00	0.04	-0.70	0.18	1.77	1.29	0.00	0.02	-0.89	0.17	1.94	1.24
11	0.00	0.06	-0.90	0.19	2.52	1.86	0.00	0.05	-1.23	0.20	2.50	1.52
22	0.00	0.06	-0.90	0.19	2.57	1.92	0.01	-0.10	1.38	-0.21	42.27	43.36
33	0.00	0.06	-0.90	0.19	2.57	1.92	0.00	-0.08	0.49	-0.03	133.98	134.36

P11D, the calculated spectra resemble some features of the experimental observation. Nonetheless, when more diffuse functions were added, the calculated results are totally different with the observations. The components in Table 4 show that the diffuse functions dominate the contribution in $d\mu_k$ when even only one set of diffuse functions was added. Thus, the discrepancy between the calculated and experimental spectra should be attributed to the wrong description of the extra electron at the B3LYP level when more diffuse functions were used. Here, we should emphasize that the previous assignment for the structure of W/D_4^-, even though correct, was based on the unconverged calculation results.[13,34] The experimental and theoretical IR spectra are in agreement with each other merely by coincidence.

The calculated IR spectra for W/$D_{5,6}^-$ were depicted in Figs. 6 and 7, respectively. At the MP2 level, the relative IR intensities again converge with one extra diffuse function. The assignment for converged spectra in the bending region is the same as that for W_4^-. The calculated spectra in this region are in agreement with the experimental observations. On the other hand, there are three bands in the stretching region. The same as in D_3^-, these bands are assigned to ν_s, ν_s' and ν_a from low to high frequency, respectively. The calculated relative intensities of ν_s and ν_s' are comparable to the experimental results. However, the intensity of ν_a is significantly overestimated by the MP2 method.

The components of $d\mu_k$ for W/$D_{5,6}^-$ in Tables 5 and 6 show that they are certainly converged when two sets of diffuse functions were added. With S33D and P33D, the largest absolute contribution of individual basis set belongs to the second outermost diffuse functions, which is consistent with the convergence of the total $d\mu_k$. For ν_b, with SmnD, the diffuse functions have the largest contribution and the valence components have considerably negative contribution, while with PmnD, the diffuse functions dominant. For ν_s, with SmnD, the valence components are the major part due to the cancellation of individual contributions from diffuse functions. However, with PmnD, the contributions from diffuse functions are dominant and the valence has the most negative contribution.

At the B3LYP level with S11D, P10D, and P11D, the calculated IR spectra in the stretching region are in agreement with experimental spectra (here the relative intensity of ν_a is lower

Table 6 Components of dynamic IR dipole moment for anionic water hexamer. N: Nuclear; C: Core basis set; V: Valence basis set; P: Polarization basis set; D: Diffuse basis set; T: Total.

	MP2						B3LYP					
m,n	N	C	V	P	D	T	N	C	V	P	D	T
						ν_b						
SmnD												
00	-0.48	-0.04	-3.90	-1.44	6.56	0.70	-0.52	-0.05	-2.31	-1.50	4.97	0.60
11	-0.19	-0.02	-3.61	-0.66	4.92	0.45	-0.51	-0.04	-5.03	-1.17	7.27	0.51
22	-0.27	-0.02	-4.35	-0.78	5.88	0.46	-0.08	-0.01	-1.39	-0.34	3.93	2.11
33	-0.27	-0.02	-4.35	-0.78	5.88	0.46	-0.43	-0.04	-3.47	-0.85	8.27	3.48
PmnD												
00	-0.50	-0.07	0.06	0.12	1.06	0.67	-0.51	-0.07	-0.22	0.10	1.27	0.58
10	-0.36	-0.05	0.11	0.07	0.70	0.47	-0.55	-0.08	-0.12	0.11	1.26	0.62
11	0.06	0.01	0.04	-0.02	0.37	0.45	-0.54	-0.07	-0.08	0.10	1.08	0.49
22	-0.03	0.00	0.06	0.00	0.40	0.43	-0.04	-0.01	-0.06	0.01	8.95	8.85
33	-0.03	0.00	0.07	0.00	0.40	0.43	-0.58	-0.08	0.00	0.11	32.11	31.55
						ν_s						
SmnD												
00	0.00	0.02	2.01	-0.55	-0.78	0.70	0.00	-0.01	0.44	-0.07	0.39	0.75
11	0.00	0.04	1.89	-0.22	0.12	1.82	0.00	0.04	1.34	-0.10	0.10	1.37
22	0.00	0.04	1.93	-0.22	0.04	1.79	0.00	0.00	-0.92	-0.16	6.25	5.18
33	0.00	0.04	1.93	-0.22	0.04	1.79	0.00	-0.05	-0.73	0.35	8.17	7.74
PmnD												
00	0.00	0.02	-1.04	0.17	1.34	0.49	0.00	-0.04	-0.12	0.01	0.81	0.67
10	0.00	0.06	-1.02	0.24	1.97	1.26	0.00	0.04	-1.35	0.24	2.14	1.07
11	0.00	0.07	-1.17	0.25	2.60	1.74	0.00	0.06	-1.61	0.27	2.60	1.31
22	0.00	0.07	-1.17	0.25	2.60	1.75	0.00	-0.03	0.83	-0.15	3.64	4.29
33	0.00	0.07	-1.17	0.25	2.60	1.75	0.01	-0.11	1.76	-0.26	14.51	15.91

than that at the MP2 level). However, in the bending region, the calculated results are quite different from the experimental counterparts. Furthermore, when more diffuse functions were added, the IR spectra are diverse in both regions. Thus, we would attribute the similarity in the stretching region to coincidence again. The detailed components in Tables 5 and 6 indicate that the diffuse functions dominate in $d\mu_k$ and become larger and larger. This result reveals that B3LYP has a questionable description of the extra electron in W/$D^-_{5,6}$.

4 Conclusions

In this work, we have examined the convergence of calculated IR spectra for W/D^-_{2-6} with respect to the number of diffuse functions at both MP2 and B3LYP levels. For the MP2 method, the convergence can be achieved with respect to the used basis sets. The converged IR spectra are in good agreement with experimental observations. It can be concluded that the MP2 method has the ability to correctly describe the extra electron in the dipole bounded systems. In contrast, the convergence has never been obtained for all clusters under investigations at the B3LYP level. The contribution of diffuse functions to the properties becomes larger with the increased number of diffuse functions. It certainly implies that it is questionable to use B3LYP to study the systems bounded with an extra electron, although such excises can be frequently found in the literature. The basis set dependence could be a useful measure to examine the applicability of some modern DFT functionals (also high level post Hartree-Fock methods), in particular, the functionals with correct asymptotic decaying as well as the doubly hybrid functionals, for such anionic water clusters.

5 Acknowledgments

This work was supported by Ministry of Science and Technology of China (Grant Nos. 2010CB923300 and 2011CB808505), Natural Science Foundation of China (Grant Nos. 20925311 and 21473166), the Fundamental Research Funds for the Central Universities (Nos. WK2090050027 and WK2310000035), and Göran Gustafsson Foundation for Research in Natural Sciences and Medicine. The Swedish

National Infrastructure for Computing (SNIC) was acknowledged for computer time.

References

1 M. Armbruster, H. Haberland and H.-G. Schindler, *Phys. Rev. Lett.*, 1981, **47**, 323–326.
2 H. Haberland, H.-G. Schindler and D. R. Worsnop, *Ber. Bunsenges. Phys. Chem.*, 1984, **88**, 270–272.
3 E. Hart and M. Anbar, *The Hydrated Electron*, Wiley-Interscience, New York, 1970.
4 P. J. Campagnola, D. J. Lavrich, M. J. DeLuca and M. A. Johnson, *J. Chem. Phys.*, 1991, **94**, 5240–5242.
5 S. T. Arnold, R. A. Morris, A. A. Viggiano and M. A. Johnson, *J. Phys. Chem. A*, 1996, **100**, 2900–2906.
6 M. K. Beyer, B. S. Fox, B. M. Reinhard and V. E. Bondybey, *J. Chem. Phys.*, 2001, **115**, 9288–9297.
7 C. Desfrançois, S. Carles and J. P. Schermann, *Chem. Rev.*, 2000, **100**, 3943–3962.
8 R. N. Barnett, U. Landman, C. L. Cleveland and J. Jortner, *J. Chem. Phys.*, 1988, **88**, 4429–4447.
9 J. V. Coe, G. H. Lee, J. G. Eaton, S. T. Arnold, H. W. Sarkas, K. H. Bowen, C. Ludewigt, H. Haberland and D. R. Worsnop, *J. Chem. Phys*, 1990, **92**, 3980–3982.
10 A. Bar-on and R. Naaman, *J. Chem. Phys.*, 1989, **90**, 5198–5199.
11 L. A. Posey and M. A. Johnson, *J. Chem. Phys.*, 1988, **89**, 4807–4814.
12 P. Ayotte, C. G. Bailey, J. Kim and M. A. Johnson, *J. Chem. Phys.*, 1998, **108**, 444–449.
13 N. I. Hammer, J.-W. Shin, J. M. Headrick, E. G. Diken, J. R. Roscioli, G. H. Weddle and M. A. Johnson, *Science*, 2004, **306**, 675–679.
14 A. E. Bragg, J. R. R. Verlet, A. Kammrath, O. Cheshnovsky and D. M. Neumark, *Science*, 2004, **306**, 669–671.
15 D. H. Paik, I.-R. Lee, D.-S. Yang, J. S. Baskin and A. H. Zewail, *Science*, 2004, **306**, 672–675.
16 C. G. Bailey, J. Kim and M. A. Johnson, *J. Phys. Chem.*, 1996, **100**, 16782–16785.
17 N. I. Hammer, J. R. Roscioli, M. A. Johnson, E. M. Myshakin and K. D. Jordan, *J. Phys. Chem. A*, 2005, **109**, 11526–11530.
18 P. Ayotte, G. H. Weddle, C. G. Bailey, M. A. Johnson, F. Vila and K. D. Jordan, *J. Chem. Phys.*, 1999, **110**, 6268–6277.
19 C. J. Tsai and K. Jordan, *Chem. Phys. Lett.*, 1993, **213**, 181–188.
20 S. B. Suh, H. M. Lee, J. Kim, J. Y. Lee and K. S. Kim, *J. Chem. Phys.*, 2000, **113**, 5273–5277.
21 R. F. Wallis, R. Herman and H. W. Milnes, *J. Mol. Spectrosc.*, 1960, **4**, 51–74.
22 K. Fox and J. E. Turner, *J. Chem. Phys.*, 1966, **45**, 1142–1144.
23 M. Mittleman and V. Myerscough, *Phys. Lett.*, 1966, **23**, 545–546.
24 J.-M. Lévy-Leblond, *Phys. Rev.*, 1967, **153**, 1–4.
25 C. A. Coulson and M. Walmsley, *Proc. Phys. Soc.*, 1967, **91**, 31–32.
26 W. B. Brown and R. E. Roberts, *J. Chem. Phys.*, 1967, **46**, 2006–2007.
27 W. Garrett, *Chem. Phys. Lett.*, 1970, **5**, 393–397.
28 O. H. Crawford, *Mol. Phys.*, 1971, **20**, 585–591.
29 S. A. Clough, Y. Beers, G. P. Klein and L. S. Rothman, *J. Chem. Phys.*, 1973, **59**, 2254–2259.
30 K. D. Jordan and J. J. Wendoloski, *Chem. Phys.*, 1977, **21**, 145–154.
31 D. M. Chipman, *J. Chem. Phys.*, 1978, **82**, 1080–1083.
32 D. M. Chipman, *J. Phys. Chem.*, 1979, **83**, 1657–1662.
33 C. Møller and M. Plesset, *Phys. Rev.*, 1934, **46**, 618–622.
34 H. M. Lee, S. Lee and K. S. Kim, *J. Chem. Phys.*, 2003, **119**, 187–194.
35 K. D. Jordan and F. Wang, *Annu. Rev. Phys. Chem.*, 2003, **54**, 367–396.
36 P. J. Stephens, F. J. Devlin, C. F. Chabalowski and M. J. Frisch, *J. Phys. Chem.*, 1994, **98**, 11623–11627.
37 K. S. Kim, S. Lee, J. Kim and J. Y. Lee, *J. Am. Chem. Soc.*, 1997, **119**, 9329–9330.
38 H. M. Lee and K. S. Kim, *J. Chem. Phys.*, 2002, **117**, 706–708.
39 H. M. Lee, S. Bum Suh and K. S. Kim, *J. Chem. Phys.*, 2003, **118**, 9981–9986.
40 H. M. Lee, S. B. Suh and K. S. Kim, *J. Chem. Phys.*, 2003, **119**, 7685–7692.
41 H. M. Lee, S. B. Suh, P. Tarakeshwar and K. S. Kim, *J. Chem. Phys.*, 2005, **122**, 044309.
42 J. M. Herbert and M. Head-Gordon, *J. Am. Chem. Soc.*, 2006, **128**, 13932–13939.
43 J. M. Herbert and M. Head-Gordon, *Proc. Natl. Acad. Sci. U. S. A.*, 2006, **103**, 14282–14287.
44 J. R. Roscioli and M. A. Johnson, *J. Chem. Phys.*, 2007, **126**, 024307.
45 J. Kim, S. B. Suh and K. S. Kim, *J. Chem. Phys.*, 1999, **111**, 10077–10087.
46 G. D. Purvis III and R. J. Bartlett, *J. Chem. Phys.*, 1982, **76**, 1910–1918.
47 J. Kim, J. Y. Lee, K. S. Oh, J. M. Park, S. Lee and K. S. Kim, *Phys. Rev. A*, 1999, **59**, R930–R933.
48 J. M. Herbert and M. Head-Gordon, *J. Phys. Chem. A*, 2005, **109**, 5217–5229.
49 K. Yagi, Y. Okano, T. Sato, Y. Kawashima, T. Tsuneda and K. Hirao, *J. Phys. Chem. A*, 2008, **112**, 9845–9853.
50 V. P. Vysotskiy, L. S. Cederbaum, T. Sommerfeld, V. K. Voora and K. D. Jordan, *J. Chem. Theory Comput.*, 2012, **8**, 893–900.
51 W. Koch and M. C. Holthausen, *A Chemist's Guide to Density Functional Theory*, Wiley-VCH Verlag GmbH, Weinheim New York, 2nd edn, 2001.
52 P. Skurski, M. Gutowski and J. Simons, *Int. J. Quantum Chem.*, 2000, **80**, 1024–1038.
53 T. Sommerfeld, *J. Chem. Phys.*, 2007, **126**, 027101.
54 R. Krishnan, J. S. Binkley, R. Seeger and J. A. Pople, *J. Chem. Phys.*, 1980, **72**, 650–654.
55 T. Clark, J. Chandrasekhar, G. W. Spitznagel and P. V. R. Schleyer, *J. Comp. Chem.*, 1983, **4**, 294–301.
56 T. H. Dunning Jr., *J. Chem. Phys.*, 1989, **90**, 1007–1023.
57 R. A. Kendall, T. H. Dunning Jr. and R. J. Harrison, *J. Chem. Phys.*, 1992, **96**, 6796–6806.
58 E. R. Davidson, *Chem. Phys. Lett.*, 1996, **260**, 514–518.
59 A. J. Sadlej, *Collect. Czech. Chem. Commun.*, 1988, **53**, 1995–2016.
60 M. J. Frisch, G. W. Trucks, H. B. Schlegel, G. E. Scuseria, M. A. Robb, J. R. Cheeseman, G. Scalmani, V. Barone, B. Mennucci, G. A. Petersson, H. Nakatsuji, M. Caricato, X. Li, H. P. Hratchian, A. F. Izmaylov, J. Bloino, G. Zheng, J. L. Sonnenberg, M. Hada, M. Ehara, K. Toyota, R. Fukuda, J. Hasegawa, M. Ishida, T. Nakajima, Y. Honda, O. Kitao, H. Nakai, T. Vreven, J. A. Montgomery, Jr., J. E. Peralta, F. Ogliaro, M. Bearpark, J. J. Heyd, E. Brothers, K. N. Kudin, V. N. Staroverov, R. Kobayashi, J. Normand, K. Raghavachari, A. Rendell, J. C. Burant, S. S. Iyengar, J. Tomasi, M. Cossi, N. Rega, J. M. Millam, M. Klene, J. E. Knox, J. B. Cross, V. Bakken, C. Adamo, J. Jaramillo, R. Gomperts, R. E. Stratmann, O. Yazyev, A. J. Austin, R. Cammi, C. Pomelli, J. W. Ochterski, R. L. Martin, K. Morokuma, V. G. Zakrzewski, G. A. Voth, P. Salvador, J. J. Dannenberg, S. Dapprich, A. D. Daniels, Ö. Farkas, J. B. Foresman, J. V. Ortiz, J. Cioslowski and D. J. Fox, *Gaussian 09 Revision B. 01*, Gaussian Inc. Wallingford CT 2009.
61 S. Obara and A. Saika, *J. Chem. Phys.*, 1986, **84**, 3963–3974.
62 M. Head-Gordon and J. A. Pople, *J. Chem. Phys.*, 1988, **89**, 5777–5786.
63 T. P. Hamilton and H. F. Schaefer III, *Chem. Phys.*, 1991, **150**, 163–171.
64 J. Gerratt and I. M. Mills, *J. Chem. Phys.*, 1968, **49**, 1719–1729.
65 J. A. Pople, R. Krishnan, H. B. Schlegel and J. S. Binkley, *Int. J. Quantum Chem.*, 1979, **16**, 225–241.

66 B. Fornberg, *Math. Comp.*, 1988, **51**, 699–760.
67 W. T. King, G. B. Mast and P. P. Blanchette, *J. Chem. Phys.*, 1972, **56**, 4440–4446.
68 J. Cioslowski, *J. Am. Chem. Soc.*, 1989, **111**, 8333–8336.
69 A. Milani and C. Castiglioni, *J. Phys. Chem. A*, 2010, **114**, 624–632.
70 R. S. Mulliken, *J. Chem. Phys.*, 1955, **23**, 1833–1840.
71 Further differentiation of Eq. 2 with respect to external electric field F reads
$$\frac{\partial \alpha}{\partial Q_k} = -\mathrm{Tr}\left(\frac{\partial^2 P}{\partial F \partial Q_k} X + \frac{\partial P}{\partial F}\frac{\partial X}{\partial Q_k}\right).$$
Thus, the dynamic Raman polarizability could be easily decomposed into different atomic basis set.
72 M. D. Halls and H. B. Schlegel, *J. Chem. Phys*, 1998, **109**, 10587–10593.
73 M. D. Halls and H. B. Schlegel, *J. Chem. Phys.*, 1999, **111**, 8819–8824.
74 F. Jensen, *J. Chem. Theory Comput.*, 2010, **6**, 2726–2735.
75 M.-C. Kim, E. Sim and K. Burke, *J. Chem. Phys.*, 2011, **134**, 171103.
76 J. P. Perdew, K. Burke and M. Ernzerhof, *Phys. Rev. Lett.*, 1996, **77**, 3865–3868.
77 A. D. Becke, *Phys. Rev. A*, 1988, **38**, 3098–3100.
78 J. P. Perdew and A. Zunger, *Phys. Rev. B*, 1981, **23**, 5048–5079.
79 H. Iikura, T. Tsuneda, T. Yanai and K. Hirao, *J. Chem. Phys.*, 2001, **115**, 3540–3544.
80 Y. Zhao and D. Truhlar, *Theor. Chem. Acc.*, 2008, **120**, 215–241.
81 T. Yanai, D. P. Tew and N. C. Handy, *Chem. Phys. Lett.*, 2004, **393**, 51–57.
82 J.-D. Chai and M. Head-Gordon, *Phys. Chem. Chem. Phys.*, 2008, **10**, 6615–6620.
83 S. Grimme, *J. Chem. Phys.*, 2006, **124**, 034108.
84 T. Sommerfeld, S. D. Gardner, A. DeFusco and K. D. Jordan, *J. Chem. Phys.*, 2006, **125**, 174301.